

Transverse expansion of (1 + 2) dimensional magneto-hydrodynamics flow with longitudinal boost invariance

A. Emamian, A. F. Kord, A. Ghaani, B. Azadegan

Department of Physics, Hakim Sabzevari University (HSU), P.O.Box 397, Sabzevar, Iran.

E-mail: a.farzaneh@hsu.ac.ir

Abstract

In the present work, we investigate the effects of magnetic field on expanding hot and dense nuclear matter as an ideal fluid. We consider QGP, on the particular case of a (1 + 2) dimensional longitudinally boost-invariant fluid expansion, in the background of an inhomogeneous magnetic field that is generated by external sources. We assume the magnetic field points in the direction perpendicular to the reaction plane, follows the power-law decay in proper time, and has two components on the transverse plane. To simplify the calculation, we suppose the investigated fluid has azimuthal symmetry, and magneto-hydrodynamic equations are described in a polar coordinate system on the transverse plane of reaction. Our results depict the space-time evolution of the transverse expansion of the fluid in the presence of an inhomogeneous external magnetic field. Ultimately, we utilize transverse velocity and correction of energy density to estimate the transverse momentum spectrum of final particles that emerge from heavy-ion collisions based on experimental data.

Keyword: Heavy-ion collisions, Magneto-hydrodynamics

1 Introduction

According to the experimental data from relativistic Heavy Ion Collisions (HICs) at RHIC and LHC, a unique form of hot and dense nuclear matter is in the initial stage of collisions created, which is ordinarily known as Quark-Gluon Plasma (QGP). It is discussed that QGP behaves more like a strongly coupled, nearly perfect fluid. The QGP phase description in terms of relativistic hydrodynamics has been fairly successful in the heavy-ion collision experiments [1–6].

One of the interesting phenomena in the heavy-ion collision is generating a strong magnetic field in the early stages of heavy-ion collision due to the spectator protons' relativistic motion. It is argued the strength of this magnetic field can be reached to the order of $eB \sim m_\pi^2 \sim 10^{18} - 10^{19} G$ in the initial stages of the collision [7–9].

The significance of EM fields on the QGP medium has been investigated for some events. For example, if the number of left- and right-handed quarks is unbalanced, a net charge current will be induced by the magnetic field. This phenomenon is called chiral magnetic effect (CME) [8, 10]. Besides, chiral magnetic wave (CMW) is another phenomenon that one could describe in terms of a chiral current induced by the magnetic field [11]. These effects could explain breaking symmetry in the angular distribution of final charged particles, and also the difference between the elliptic flow of π^+ and the elliptic flow of π^- [12]. Some phenomena may be explained in terms of an electric field in the early stage of QGP, such as the chiral electric separation effect and chiral Hall-separation effect. One can find more references and information in [13–16].

To study the phenomena mentioned above in the relativistic hydrodynamic framework, one needs to solve the Maxwell equations and the conservation equations for the energy-momentum tensor. The

model is called the relativistic magneto-hydrodynamic (RMHD). There is an open question about the effect of the magnetic field on the evaluation of QGP. It is known the magnetic field generated in heavy-ion collisions decays very fast in the vacuum [8], but its decay becomes more slowly in the presence of an electrically conducting media [17–20]. Therefore, there is still a challenge of how magnetic field may have significant consequences on the quark-gluon matter dynamics. Simplified studies have been done about a magnetic field’s possible effect on QGP evolution [18, 19]. Besides, more numerical advance methods have been used in the framework of the relativistic magneto-hydrodynamic (RMHD) or a (1+3) dimensional partonic cascade BAMPS (Boltzmann Approach to Multi-Parton Scatterings) [21–24].

Moreover, several works have been published in a parallel analytical approach, with longitudinal boost invariance and an external transverse magnetic field [25–28]. Solutions have been found a (1+1) dimensional Bjorken flow within ideal transverse RMHD. Furthermore, in ref [26], the magnetization property has been added and studied. The (1+2) dimensional expansion of a perfect fluid in the presence of an external magnetic field has been examined in [29], where the external magnetic field has been pointed in the transverse Cartesian coordinate y direction. Besides, all hydrodynamic quantities (P, ϵ, T, B^2) have been dependent on proper time (τ) and Cartesian coordinates (x, y). The model has been called reduced MHD.

In an earlier paper [28], we have considered an ideal fluid in the presence of a weak external inhomogeneous magnetic field pointing along the ϕ direction. Besides, we have discussed the expansion in a cylindrical coordinate system. Because of the particular choice of the magnetic field (ϕ direction), we have only considered central collisions. The decay of the magnetic field has been assumed as $\tau^{n/2}$ with τ being proper time and n being an arbitrary negative number. The analytical solutions have been only obtained for $n = -1$ and $n = -\frac{4}{3}$. In recent work, we shall modify the previous model and consider a weak external inhomogeneous magnetic field pointing along the arbitrary direction in the transverse plane; therefore, the magnetic field has two components b_ϕ and b_r in a cylindrical coordinate system. Thus, we investigate the (1+2) dimensional expansion of an ideal perfectly conducting fluid in the hydrodynamic framework in the presence of the magnetic field. For simplicity, we ignore magnetization and dissipative effects. It is known for a perfectly conducting fluid the evolution of energy density, and magnetic field are decoupled because of frozen-flux theorem [26, 30]. However, we follow the scenarios in refs [25–27], and consider a conducting fluid in the presence of an external magnetic field with power decay low as $\tau^{n/2}$ and n being a negative number of the fluid. In the heavy-ion collisions, we mostly consider outlines in which the magnetic field decays more rapidly than in the ideal-MHD case, and energy density decays more slowly than in the ideal-MHD case. The ideal-MHD point corresponds to $n = -2$.

The paper is organized as follows. In section 2, we illustrate the ideal relativistic magneto-hydrodynamic framework in the case of a plasma. Next, we display our perturbative approach and obtain analytical solutions. The general results are discussed in section 3. Then, we calculate the transverse momentum spectrum and compare it with experimental data obtained in RHIC. The last section relates the conclusions and subsequent issues.

2 Ideal relativistic magneto-hydrodynamic in the transverse expansion

We present a brief preview of our formalism to describe the interaction of matter and electromagnetic fields in plasma. We assume there is only an external magnetic field interacted with QGP matter. The external magnetic field is generated by the charged spectators. It is known external fields may induce internal electromagnetic fields dictated by Maxwell’s equations. To give a complete description of matter, one should solve both Maxwell’s equations and the conservation equations together. However, in the present work, we ignore the induced internal electromagnetic fields and only investigate the effects of the external magnetic field on QGP matter. Besides, we

assume an arbitrary function for the magnetic field because external sources create it, and we only solve the conservation equations.

We discuss the case of an ideal non-resistive plasma with massless particles. Besides, the set of equations can be closed by incorporating a thermodynamic EoS assumed the pressure is merely proportional to the energy density as $P = \kappa\epsilon$ where κ is constant. Finally, we present the the energy-momentum conservation equations for an ideal fluid in the presence of an external magnetic field in the RMHD framework [31, 32].

The covariant form of energy-momentum conservation equations is given by:

$$d_\mu(T_F^{\mu\nu} + T_{EM}^{\mu\nu}) = 0 \quad (1)$$

where

$$T_F^{\mu\nu} = (\epsilon + P)u^\mu u^\nu + P g^{\mu\nu} \quad (2)$$

$$T_{EM}^{\mu\nu} = b^2 u^\mu u^\nu + \frac{1}{2} b^2 g^{\mu\nu} - b^\mu b^\nu \quad (3)$$

Here ϵ and P are the energy density and pressure of the fluid, respectively, and b^μ is the magnetic field four-vector with modulus $b^\mu b_\mu = b^2$. The metric tensor in a flat spacetime is $g_{\mu\nu} = \text{diag}\{-, +, +, +\}$, and so that $u_\mu = \gamma(1, \vec{v})$ is the four-velocity of fluid satisfying $u^\mu u_\mu = -1$.

By introducing the orthogonal projector to the fluid four-velocity as $\Delta^{\mu\nu} = g^{\mu\nu} + u^\mu u^\nu$, one can rewrite the conservation equation alongside the parallel and perpendicular directions to u_ν . They are:

$$u_\nu d_\mu(T_F^{\mu\nu} + T_{EM}^{\mu\nu}) = 0 \implies D(\epsilon + \frac{b^2}{2}) + (\epsilon + P + b^2)\Theta + u_\nu b^\mu (d_\mu b^\nu) = 0 \quad (4)$$

and

$$\Delta_{\alpha\nu} d_\mu(T_F^{\mu\nu} + T_{EM}^{\mu\nu}) = 0 \implies (\epsilon + P + b^2)Du_\alpha + \nabla_\alpha(P + \frac{b^2}{2}) - d_\mu(b^\mu b_\alpha) - u_\alpha u_\nu d_\mu(b^\mu b^\nu) = 0 \quad (5)$$

where:

$$D = u^\mu d_\mu, \quad \Theta = d_\mu u^\mu, \quad \nabla_\alpha = \Delta_{\alpha\nu} d^\nu \quad (6)$$

In relativistic heavy-ion collisions, the nuclei are accelerated toward each other in the center-of-mass frame with velocities near the light speed. However, all the motion is longitudinal before the collision, and it may still be assumed to remain in the longitudinal direction. Moreover, the fluid is assumed with a finite transverse size and expands both in the longitudinal and radial direction. Thus the four-velocity for an ideal fluid following the Bjorken expansion along the z direction and moving in the transverse plane only in the r direction in a cylindrical coordinate becomes:

$$u_\mu = \frac{1}{\sqrt{1 - u_z^2 - u_r^2}}(1, u_r, 0, u_z) \quad (7)$$

where u_r and u_z are the radial and longitudinal components, and u_ϕ is zero. Besides, the boost invariance of the Bjorken expansion allows us to restrict the discussion to the $z = 0$ plane where symmetry reasons impose $u_z = 0$. As we know, it is more advantageous to work in Milne coordinates, $x_\mu = (\tau, r, \phi, \eta)$, such that:

$$\tau = \sqrt{t^2 - z^2}, \quad \eta = \frac{1}{2} \ln \frac{t+z}{t-z}, \quad \phi = \tan^{-1}(y/x), \quad r^2 = x^2 + y^2 \quad (8)$$

and the metric for these coordinates is parameterized as $g_{\mu\nu} = \text{diag}\{-1, 1, r^2, \tau^2\}$. The covariant derivatives in Eqs. (4) and (5) are defined as:

$$\begin{aligned} d_\mu A^\nu &= \partial_\mu A^\nu + \Gamma_{\mu\rho}^\nu A^\rho \\ d_\mu(A^\nu A^\alpha) &= \partial_\mu(A^\nu A^\alpha) + \Gamma_{\mu\sigma}^\nu A^\sigma A^\alpha + \Gamma_{\mu\sigma}^\alpha A^\nu A^\sigma \end{aligned} \quad (9)$$

where the only non-zero Cristoffel symbols according to the following definition:

$$\Gamma_{jk}^i = \frac{1}{2} g^{im} \left(\frac{\partial g_{mj}}{\partial x^k} + \frac{\partial g_{mk}}{\partial x^j} - \frac{\partial g_{jk}}{\partial x^m} \right). \quad (10)$$

are $\Gamma_{\eta\eta}^\tau = \tau$, $\Gamma_{\phi\phi}^r = -r$, $\Gamma_{r\phi}^\phi = \frac{1}{r}$, $\Gamma_{\tau\eta}^\eta = \frac{1}{\tau}$.

In order to simplify our calculation, we apply the longitudinal boost invariance and rotational symmetry around the beamline. The assumptions of boost invariance and rotational symmetry around the beamline imply that none of the quantities depends on η and ϕ coordinates. Consequently, we expect that all the quantities of interest solely rely on the transverse radial r and τ coordinate in the (τ, r, ϕ, η) coordinate system. The assumption of boost invariance is approximate correct near mid rapidity [32]. Moreover, it is known collisions with significant impact parameters break the rotational symmetry. In this case, to describe systems without rotational symmetry, one needs to include three additional quantities: the shear and bulk viscosities and the thermal conductivity, respectively [33]. However, a general calculation, including the viscosities, is out of the scope of this work.

To improve the previous work of two of the authors [28], due to non-central collisions and asymmetric charge distribution, we suppose that the magnetic field is perpendicular to the reaction plane pointing along the r and ϕ directions. However, we assume the magnitude of the magnetic field is independent of ϕ , but it is shown each component of the magnetic field can be dependent on the ϕ coordinate.

We also ignore the Maxwell equations and assume the external sources govern the dynamics of the magnetic field. Then, we solve the conservation equations perturbatively and analytically. It is known the magnitude of the magnetic field drops rapidly concerning time because fast velocities of the charged spectators (as sources for the external magnetic field) fly away along the beam direction [8, 17]. Thus, the energy density of the magnetic field could be suppressed by the energy density of the fluid at some initial time after collisions [27]. Therefore, we follow the perturbative scenario which has been introduced in [27], and consider $\frac{b^2}{\epsilon} \ll 1$. Hence, one can ignore Maxwell equations, and external sources dictate the dynamics of the magnetic field. Furthermore, as been discussed by authors in [27], one could ignore the nonlinear effects in b^2 at a perturbative treatment despite that they may be necessary in very early times.

We shall investigate perturbative solutions of the conservation equations in the presence of an external weak inhomogeneous magnetic field pointing along the r and ϕ directions in an inviscid fluid with a high enough electrical conductivity. The initial setup of our study is given by:

$$u_\mu = (1, \lambda^2 u_r, 0, 0), \quad b_\mu = (0, \lambda b_r, \lambda r b_\phi, 0), \quad \epsilon = \epsilon_0(\tau) + \lambda^2 \epsilon_1(\tau, r) \quad (11)$$

Here $\epsilon_0(\tau) = \frac{\epsilon_c}{\tau^{4/3}}$, and τ is rescaled by an initial time τ_0 . ϵ_c is the energy density at proper time τ_0 . Also, λ is an expansion parameter, which will be set to unity at the end of calculations. Besides, in our calculations, we implicitly rescale r by τ_0 . By substituting the above condition in the energy conservation (4) and Euler equation (5), we have obtained three coupled differential equations. Up

to order $O(\lambda^2)$, we have:

$$\partial_\tau \epsilon_1 - \frac{4\epsilon_c}{3\tau^{4/3}} \left(\frac{u_r}{r} + \frac{\partial u_r}{\partial r} \right) + \frac{4\epsilon_1}{3\tau} + \frac{b^2}{\tau} + \frac{1}{2} \partial_\tau b^2 = 0 \quad (12)$$

$$\partial_r (b_r b_\phi) + \frac{2b_r b_\phi}{r} + \frac{2b_\phi}{r} \partial_\phi b_\phi = 0 \quad (13)$$

$$\partial_r \epsilon_1 - \frac{4\epsilon_c}{\tau^{4/3}} \partial_\tau u_r + \frac{4\epsilon_c}{3\tau^{7/3}} u_r - \frac{3}{r} (b_r^2 - b_\phi^2) + \frac{3}{2} \partial_r b^2 - 3\partial_r b_r^2 - \frac{3}{r} \partial_\phi (b_\phi b_r) = 0 \quad (14)$$

Assuming rotational symmetry around the beamline:

$$\partial_\phi b^2(\tau, r) = 0 \quad (15)$$

and using the method of the separation of variables, we have solved Eqs. (13) and (15). Then, b_r , b_ϕ , and b^2 are quickly achieved as follow:

$$b_r(\tau, r, \phi) = \sum_{l=-2}^{\infty} C_l(\tau) r^{\frac{l}{2}} [A_l \cos(\frac{(l+2)\phi}{2}) + B_l \sin(\frac{(l+2)\phi}{2})] \quad (16)$$

$$b_\phi(\tau, r, \phi) = \sum_{l=-2}^{\infty} C_l(\tau) r^{\frac{l}{2}} [B_l \cos(\frac{(l+2)\phi}{2}) - A_l \sin(\frac{(l+2)\phi}{2})] \quad (17)$$

$$\begin{aligned} b^2(\tau, r) &= \sum_{l=-2}^{\infty} C_l(\tau) r^l \{ [A_l \cos(\frac{(l+2)\phi}{2}) + B_l \sin(\frac{(l+2)\phi}{2})]^2 \\ &\quad + [B_l \cos(\frac{(l+2)\phi}{2}) - A_l \sin(\frac{(l+2)\phi}{2})]^2 \} \\ &= \sum_{l=-2}^{\infty} C'_l(\tau) r^l = f(r, \tau) \end{aligned} \quad (18)$$

where $l \geq -2$ are real numbers, and C_l, A_l, B_l and C'_l are expansion constants. These expansion coefficients must be obtained according to the physical condition of the problem. According to the existing conditions in the case of an external magnetic field, all coefficients with index $l < 0$ should be zero. Then, we substitute b_r, b_ϕ , and b^2 from above results in Eqs. (12) and (14), and obtain:

$$\partial_\tau \epsilon_1 - \frac{1}{3\tau r} \frac{\partial}{\partial r} \left(\frac{4\epsilon_c r u_r}{\tau^{1/3}} \right) + \frac{4\epsilon_1}{3\tau} + \frac{b^2}{\tau} + \frac{1}{2} \partial_\tau b^2 = 0 \quad (19)$$

$$\partial_r \epsilon_1 - \frac{1}{\tau r} \frac{\partial}{\partial \tau} \left(\frac{4\epsilon_c r u_r}{\tau^{1/3}} \right) = 0 \quad (20)$$

Interestingly, using results in Eqs. (16)-(18) we could simplify Eqs. (12), (14) as Eqs. (19) and (20). One could combine the above equations, and obtains a partial differential equation depending on $u_r(\tau, r)$ and $b^2(\tau, r)$:

$$\begin{aligned} &\frac{3r^2 \tau^{7/3}}{4\epsilon_c} \partial_r b^2(\tau, r) + \frac{3r^2 \tau^{10/3}}{8\epsilon_c} \partial_r \partial_\tau b^2(\tau, r) - r^2 \tau^2 \partial_\tau^2 u_r(\tau, r) + 3r^2 \tau^2 \partial_\tau u_r(\tau, r) \\ &- r^2 \tau \partial_\tau u_r(\tau, r) + r^2 u_r(\tau, r) - r\tau^2 \partial_r u_r(\tau, r) + \tau^2 u_r(\tau, r) = 0. \end{aligned} \quad (21)$$

This equation describes the dynamical evolution of the transverse velocity of the fluid in the presence of an external magnetic field according to our initial setup Eq. (11), and its solution directs us to explain the fluid velocity $u_r(\tau, r)$ in terms of the cylindrical radial coordinate.

2.1 Analytical solution

To solve Eq. (21), we first assume $b^2(\tau, r) = 0$ condition and obtain the general solution for the homogeneous partial differential equation by the manner of separation of variables. The general solution is given by:

$$u_r^h(\tau, r) = \sum_m \left(A_1^m J_1(mr) + A_2^m Y_1(mr) \right) \times \left(\tau^{2/3} A_3^m J_{\frac{1}{3}}(m\tau/\sqrt{3}) + \tau^{2/3} A_4^m Y_{\frac{1}{3}}(m\tau/\sqrt{3}) \right) \quad (22)$$

where m can be real or imaginary numbers and $A_{1,2,3,4}^m$ are integration constants. To find the solution for $b^2(\tau, r) \neq 0$, we make some assumptions and converting the partial differential equation into the summation of the solution of ordinary differential equations. We consider $b^2(\tau, r)$ into a series based on the r -dependence part of the solution and assume the time dependence of $b^2(\tau, r)$ behavior as τ^n with $n < 0$ which nearly represents the decay of magnetic field in heavy-ion collisions [25–27]:

$$b^2(\tau, r) = \sum_m \tau^n B_m^2 f(mr) \quad (23)$$

here B_m^2 are constants. Also, the following ansatz for radial velocity is considered:

$$u_r(\tau, r) = \sum_m \left(a_m(\tau) J_1(mr) + b_m(\tau) Y_1(mr) \right) \quad (24)$$

It is known that initial condition $u_r(\tau = 0, r) = 0$ leads to $b_m(\tau) = 0$. Substituting the Eqs. (23) and (24) into Eq. (21), we obtain:

$$J_1(mr) \left((m^2 \tau^2 + 1) a_m(\tau) + 3\tau^2 a_m''(\tau) - \tau a_m'(\tau) \right) + \frac{3m(n+2)B_m^2 \tau^{n+\frac{7}{3}}}{8\epsilon_c} f'(mr) = 0 \quad (25)$$

We can reach the following ordinary differential equation for the function $f(mr)$ by separation of variables:

$$f'(mr) = -J_1(mr) \quad (26)$$

its general solution becomes:

$$f(mr) = c_1 + J_0(mr) \quad (27)$$

For simplicity, we impose $c_1 = 0$, but in a realistic situation, one should obtain it from physical conditions on the magnetic field. However, the magnetic field should be prominent at $r = 0$. Using Eqs. (23) and (27), we can expand the $b^2(\tau, r)$ in terms of zero-order Bessel functions as following:

$$b^2(\tau, r) = \sum_m \tau^n B_m^2 J_0\left(\alpha_{0m} \frac{r}{a}\right) \quad (28)$$

where the coefficients B_m^2 are given by:

$$B_m^2 = \frac{2}{a^2 [J_1(\alpha_{0m})]^2} \int_0^a r J_0\left(\alpha_{0m} \frac{r}{a}\right) b^2(\tau, r) dr \quad (29)$$

here α_{0m} is the m th zero of J_0 .

Besides, the transverse velocity is given by:

$$u_r(\tau, r) = \sum_m a_m(\tau) J_1(mr) \quad (30)$$

Thus, the coefficients $a_m(\tau)$ is obtained by solving the following ordinary differential equation:

$$3\tau^2 a_m''(\tau) - \tau a_m'(\tau) + (m^2 \tau^2 + 1)a_m(\tau) - \frac{3m(n+2)B_m^2 \tau^{n+\frac{7}{3}}}{8\epsilon_c} = 0 \quad (31)$$

and the analytical solution is:

$$\begin{aligned} a_m(\tau) = & \tau^{2/3} \left(c_1^m J_{\frac{1}{3}}\left(\frac{m\tau}{\sqrt{3}}\right) + c_2^m Y_{\frac{1}{3}}\left(\frac{m\tau}{\sqrt{3}}\right) \right) + \frac{3m\tau^{n+\frac{7}{3}}B_m^2}{16\epsilon_c(3n+4)} \\ & \left(3(n+2) {}_0F_1\left[\frac{4}{3}, -\frac{1}{12}m^2\tau^2\right] {}_pF_q\left[\left\{\frac{n}{2} + \frac{2}{3}\right\}, \left\{\frac{2}{3}, \frac{n}{2} + \frac{5}{3}\right\}, -\frac{1}{12}m^2\tau^2\right] - (3n+4) \right. \\ & \left. {}_0F_1\left[\frac{2}{3}, -\frac{1}{12}m^2\tau^2\right] {}_pF_q\left[\left\{\frac{n}{2} + 1\right\}, \left\{\frac{4}{3}, \frac{n}{2} + 2\right\}, -\frac{1}{12}m^2\tau^2\right] \right) \end{aligned} \quad (32)$$

The transverse velocity is completely determined if constants c_1^m and c_2^m are fixed. We can find c_1^m and c_2^m by initial condition at $\tau \rightarrow \infty$. Since $b^2(\infty, r) \rightarrow 0$, we expect $u_r(\infty, r) \rightarrow 0$. By making late-time expansion of $u_r(\tau, r)$, one finds that this takes the asymptotic form as $f(\tau)\tau^{1/6}$ where $f(\tau)$ is an oscillatory function. To prevent divergent transverse velocity, one has to choose the coefficient of $\tau^{1/6}$ equal to zero. The solutions satisfying the initial condition at $\tau \rightarrow \infty$ are written as follows:

$$\begin{aligned} c_1^m &= \frac{\pi^2 2^{n-\frac{7}{3}} 3^{\frac{n}{2}+\frac{1}{3}} B_m^2 m^{-n-\frac{2}{3}} \left(\csc\left(\frac{\pi n}{2}\right) + 2 \sec\left(\frac{1}{6}(3\pi n + \pi)\right) \right)}{\epsilon_c \Gamma\left(-\frac{n}{2} - 1\right) \Gamma\left(\frac{1}{3} - \frac{n}{2}\right)} \\ c_2^m &= -\frac{\pi 2^{n-\frac{7}{3}} 3^{\frac{n}{2}+\frac{5}{6}} B_m^2 m^{-n-\frac{2}{3}} \Gamma\left(\frac{n}{2} + 2\right)}{\epsilon_c \Gamma\left(\frac{1}{3} - \frac{n}{2}\right)} \end{aligned} \quad (33)$$

After finding $u_r(\tau, r)$ we could obtain the modified energy density from Eq. (20). It is given by:

$$\epsilon_1(\tau, r) = \sum_m h^m(\tau) - \sum_m \frac{4\epsilon_c(1 - J_0(mr))(a_m(\tau) - 3\tau a_m'(\tau))}{3m\tau^{7/3}} \quad (34)$$

In the above equation, $h^m(\tau)$ is the constant of integration which is determined by solving Eq. (19):

$$h^m(\tau) = \frac{\int_1^\tau \left(\frac{4}{3}\epsilon_c m a_m(s) - \frac{1}{2}B_m^2(n+2)s^{n+\frac{1}{3}} \right) ds}{\tau^{4/3}} \quad (35)$$

Finally, replacing $a_m(\tau)$ and its derivative into Eq. (34) lead us to determine the modified energy density as:

$$\begin{aligned} \epsilon_1(\tau, r) = & \sum_m h^m(\tau) - \sum_m \frac{4\epsilon_c(1 - J_0(mr))}{3\tau^{7/3}m} \left(-\sqrt{3}\tau^{5/3}m \left(c_1^m J_{-\frac{2}{3}}\left(\frac{m\tau}{\sqrt{3}}\right) + c_2^m Y_{-\frac{2}{3}}\left(\frac{m\tau}{\sqrt{3}}\right) \right) \right. \\ & + \frac{1}{64\epsilon_c} m \tau^{n+\frac{7}{3}} B_m^2 \left(-m^2 \tau^2 {}_0F_1\left[\frac{5}{3}, -\frac{1}{12}\tau^2 m^2\right] {}_pF_q\left[\left\{\frac{n}{2} + 1\right\}, \left\{\frac{4}{3}, \frac{n}{2} + 2\right\}, -\frac{1}{12}\tau^2 m^2\right] \right. \\ & \left. \left. - \frac{8(n+2) {}_0F_1\left[\frac{1}{3}, -\frac{1}{12}\tau^2 m^2\right] {}_pF_q\left[\left\{\frac{n}{2} + \frac{2}{3}\right\}, \left\{\frac{2}{3}, \frac{n}{2} + \frac{5}{3}\right\}, -\frac{1}{12}\tau^2 m^2\right] \right)}{3n+4} \right) \end{aligned} \quad (36)$$

Note that the above solutions of $u_r(\tau, r)$ and $\epsilon_1(\tau, r)$ are invalid for $n = -4/3$, which can be observed from the divergence in the inhomogeneous solution Eq. (30) and (36). For this particular

case, the solutions are shown in the following expressions:

$$\begin{aligned}
u(\tau, r) = & \sum_m \frac{\pi m^{2/3} \Gamma(\frac{1}{3}) B_m^2}{8 \cdot 2^{2/3} \epsilon_c} \left(\frac{1}{3^{4/3}} \tau^{2/3} J_{\frac{1}{3}}\left(\frac{m\tau}{\sqrt{3}}\right) - \frac{1}{3^{5/6}} \tau^{2/3} Y_{\frac{1}{3}}\left(\frac{m\tau}{\sqrt{3}}\right) \right) \\
& + \frac{\pi m \tau B_m^2}{288 \epsilon_c \Gamma(\frac{4}{3})^2 \sqrt[3]{m\tau}} \left(-2^{2/3} \sqrt[3]{3} \Gamma(\frac{1}{3}) (m\tau)^{2/3} J_{\frac{1}{3}}\left(\frac{m\tau}{\sqrt{3}}\right) {}_pF_q\left[\left\{\frac{1}{3}\right\}, \left\{\frac{4}{3}, \frac{4}{3}\right\}, -\frac{1}{12} m^2 \tau^2\right] \right. \\
& + 2^{2/3} 3^{5/6} \Gamma(\frac{1}{3}) (m\tau)^{2/3} Y_{\frac{1}{3}}\left(\frac{m\tau}{\sqrt{3}}\right) {}_pF_q\left[\left\{\frac{1}{3}\right\}, \left\{\frac{4}{3}, \frac{4}{3}\right\}, -\frac{1}{12} m^2 \tau^2\right] \\
& \left. - 4 \sqrt[3]{2} 3^{2/3} \Gamma(\frac{4}{3})^2 J_{\frac{1}{3}}\left(\frac{m\tau}{\sqrt{3}}\right) G_{1,3}^{2,0}\left(\frac{m^2 \tau^2}{12} \middle| \begin{matrix} 1 \\ 0, 0, \frac{1}{3} \end{matrix} \right) \right) \quad (37)
\end{aligned}$$

$$\begin{aligned}
\epsilon_1(\tau, r) = & \sum_m h^m(\tau) - \sum_m \frac{4\epsilon_c(1 - J_0(mr))}{3\tau^{7/3} m} \left(-\frac{\pi m^{5/3} \tau^{5/3} \Gamma(\frac{1}{3}) B_m^2}{24 \cdot 2^{2/3} \sqrt[3]{3} \epsilon_c} \right. \\
& \left(\sqrt{3} J_{-\frac{2}{3}}\left(\frac{m\tau}{\sqrt{3}}\right) - 3 Y_{-\frac{2}{3}}\left(\frac{m\tau}{\sqrt{3}}\right) \right) + \frac{\pi (m\tau)^{5/3}}{48 \cdot 2^{2/3} 3^{5/6} \epsilon_c \Gamma(\frac{4}{3})^2} (\sqrt[3]{2} \sqrt[3]{3} (m\tau)^{2/3} \\
& \Gamma(\frac{1}{3}) (\sqrt{3} J_{-\frac{2}{3}}\left(\frac{m\tau}{\sqrt{3}}\right) - 3 Y_{-\frac{2}{3}}\left(\frac{m\tau}{\sqrt{3}}\right)) {}_pF_q\left[\left\{\frac{1}{3}\right\}, \left\{\frac{4}{3}, \frac{4}{3}\right\}, -\frac{1}{12} m^2 \tau^2\right] \\
& \left. + 12 \Gamma(\frac{4}{3})^2 J_{-\frac{2}{3}}\left(\frac{m\tau}{\sqrt{3}}\right) G_{1,3}^{2,0}\left(\frac{m^2 \tau^2}{12} \middle| \begin{matrix} 1 \\ 0, 0, \frac{1}{3} \end{matrix} \right) \right) \quad (38)
\end{aligned}$$

We should consider that in the above equations, m has to be replaced by α_{0m}/a , and one should calculate the integral in Eq. (35) numerically.

Moreover, for $n = -2$, the evolution of energy density and magnetic field are decoupled. One can see from Eq. (25) that the transverse velocity evolution is also decoupled. In this case, the velocity has just the homogeneous solutions, which are assumed to be zero. Thus, the energy correction and the transverse velocity profile is zero.

3 Results and discussions

This section will present our results numerically to understand the space-time evolution of quark-gluon plasma in a heavy-ion collision from our perturbative solutions. We would like to present transverse velocity $v_r(\tau, r) = \frac{u^r}{u^\tau}$ and the correction energy density ϵ_1 numerically. It is known the typical magnetic field produced in Au-Au peripheral collisions at $\sqrt{s_{NN}} = 200 \text{ GeV}$ is estimated $|eB| \approx 5 \sim 10 m_\pi^2$ at $\tau = 0$ after a RHIC collision. Assuming the magnitude of the initial energy density of the medium $\epsilon_c = T_0^4 \approx (300 \text{ MeV})^4$ at the initial proper time $\tau_0 = 0.6 \text{ fm}$, and also assuming the initial electromagnetic field reduce to ten times smaller at $\tau = 0.6 \text{ fm}$, one finds $B^2/\epsilon_c \approx 0.17 \sim 0.68$ [27]. Here, we consider $m_\pi \approx 150 \text{ MeV}$ and $e^2 = 4\pi/137$. In our calculations, we have assumed $B^2/\epsilon_c = 0.6$. Note that in our calculations, any change in the ratio B^2/ϵ_c will only scale the solutions.

3.1 Numerical solutions

In order to analyze our perturbative solutions and also obtain some phenomenological insights from them, we consider the following profile of the magnetic field:

$$b^2(\tau, r) = B_c^2 \tau^n e^{-\frac{r^2}{r_0^2}} \quad (39)$$

where we assumed the magnetic profile is maximum at $r = 0$; besides, the coefficients r_0 and B_c are free parameter. So here, $r_0 > 0$ characterizes the spatial width of the magnetic field. This

assumed profile allows us to reproduce b^2 via a series of Bessel functions as shown in Eq. (28). The first twenty coefficients B_m^2 calculated according to of Eq. (29) for $r_0 = 1$ are:

$$B_c^2\{0.118491,0.259315,0.364628,0.423534,0.434975,0.40637,0.350437,0.281338,0.211409,0.149238,0.0992222,0.0622491,0.0369036,0.0206963,0.0109896,0.0055289,0.002637,0.00119289,0.000512007,0.000208585\}.$$

To reproduce the assumed external magnetic profile from Eq. (39), taking the first twenty terms of series in the calculation is enough. Note that in all of the following figures, τ , r , and v_r are dimensionless, and the dimension of ϵ_1 is GeV/fm^3 . We remind the reader that τ and r are rescaled by τ_0 .

In the left panel of Fig. 1, we show a comparison between the approximated magnetic field in the Bessel series and the assumed magnetic profile Eq. (39) at $\tau = 1$ and $r_0 = 1$. In the right panel of Fig. 1, the assumed magnetic profile is plotted as a function of r for different values of r_0 . As the value of r_0 increases, the external magnetic field is distributed over a broader area of the transverse plane. In reality, the spatial distribution of the magnetic field depends on the impact parameters of peripheral collisions. In the following calculations, we choose $r_0 = 1$.

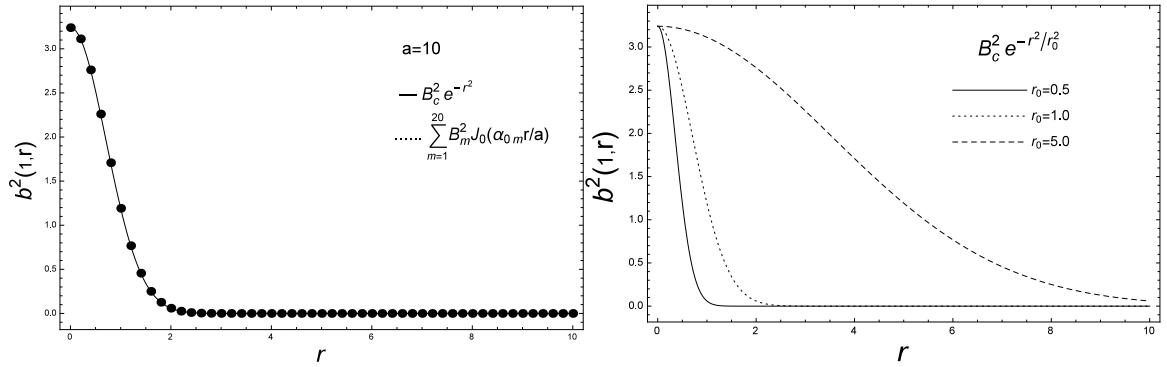


Figure 1: In the left panel, there is a comparison between the approximated b^2 in the Bessel series (dotted curve) and the assumed external magnetic field (solid curve) at $\tau = 1$ and $r_0 = 1$. In the right panel, the assumed external magnetic field is plotted for three different values of r_0 .

In order to demonstrate the effects of the magnetic field on the fluid velocity and the modified energy density, we plot the transverse fluid velocity and the modified energy density where we have chosen $B_c^2/\epsilon_c = 0.6$. As two examples, we plot the transverse fluid velocity and the modified energy density for two different values of $n = -1, -3$ at either τ or fixed r , respectively. In Figs. 2 and 3, the transverse flow $v_r(\tau, r) = \frac{u_r}{u^\tau} = -u_r$ is displayed at fixed τ and fixed r , respectively. Fig. 2 shows that the magnitude of the transverse flow ($|v_r(\tau = 1, r)|$) increases from $r = 0$, has a maximum at intermediate r and then gradually decreases with r . Fig. 3 shows $|v_r(\tau, r = 1)|$ decreases with respect to proper time due to the decay of the magnetic field.

in Figs. 4 and 5 we display v_r in terms of r and τ . Here the horizontal axis and vertical axis correspond to r and τ , respectively. Fig. 4 shows v_r is pointing inward in the medium for the case $n = -1$. However, Fig. 5 shows v_r is pointing outward in the medium for the case $n = -3$. one could conclude the external magnetic field causes the transverse compression of fluid for the case $n = -1$, and the transverse expansion of the fluid for the case $n = -3$. We should mention that the flow expands longitudinally accordingly to the Bjorken expansion, and it is not shown here. Besides, the transverse flow is more prominent around $r = 1$ as shown in Figs. 4 and 5.

In Fig. 6, and Fig. 7, we make further comparisons for $v_r(\tau, r)$ at either fixed r or fixed τ for the cases $n = -1$ and $n = -3$. They show $|v_r(\tau, r)|$ becomes smaller in late times specially For $n = -3$ because of faster decay of the magnetic field.

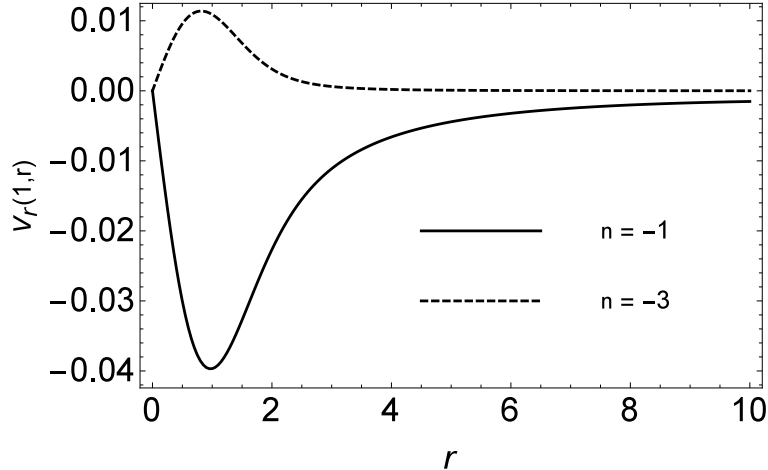


Figure 2: The transverse fluid velocity $v_r(\tau, r)$ in terms of cylindrical radial coordinate r is plotted for two different values of $n = -1, -3$ at $\tau = 1$.

Figs. 8 and 9 indicate the correction of energy density $\epsilon_1(\tau, r)$ in terms of the radial coordinate r for different values of τ and in terms of τ for different magnitudes of r in the case $n = -1$ and $n = -3$, respectively. We remind the reader that the total energy density is $\epsilon = \epsilon_0 + \epsilon_1(\tau, r)$ and the second term is truly affected by the magnetic field. From Figs. 8 and 9 For $n = -1$, we deduce that the medium system's element flows into the medium's core, and the energy density decreases. In fact, the medium loses its energy in the form of magnetic field radiation. However, for $n = -3$, the magnetic field can give the additional contribution of energy to the medium to expand it in the transverse plane.

In Fig. 10, and Fig. 11 we show further comparisons for the correction of energy density $\epsilon_1(\tau, r)$ in terms of radial coordinate r for different values of τ and in terms of τ for different magnitudes of r for cases $n = -1$ and $n = -3$. We see $\epsilon_1(\tau, r)$ is almost negative for the case $n = -1$, and positive for the case $n = -3$.

In Fig. 12, and Fig. 13, we make further comparisons for $v_r(\tau, r)$ at either fixed r or fixed τ for the cases $n < -2$ and $n > -2$. As shown in Fig. 12, when $|n|$ increases, $|v_r|$ at fixed r becomes smaller in any times. Furthermore, as shown in Fig. 12 at $\tau = 1$, we find that the $|v_r|$ first increase from $r = 0$ and then turn over at intermediate r and gradually decrease with r . For $n > -2$, the velocity profile has a similar shape compared with the cases for $n < -2$, while the direction becomes negative. Considering cases $n > -2$, the fireball system contracts in the transverse plane, but for $n < -2$ the medium expands in the transverse plane. Moreover, for the case $n = -2$ which is corresponded to the ideal-MHD the medium is stable in the transverse plane ($v_r = 0$). We see a change of the direction of the transverse velocity for $n < -2$ or $n > -2$. The transverse flow which is created by a external magnetic field points inward for $n > -2$ and outward for $n < -2$, respectively. In the case $n = -2$ the transverse flow created by the magnetic field is vanished. It is interesting if one considers n depending on the properties of the fluid specially the electric conductivity (σ). Thus, we could consider the case $n = -2$ a perfect fluid with σ goes to infinity. In this case, the decay of the magnetic field is correspond to $\frac{1}{\tau}$. Besides, the evolution of energy density and magnetic field are decoupled. In the case of $n < -2$, one could assume the fluid has a finite electric conductivity, and as $|n|$ increases σ goes to zero. Besides, the magnetic field decays faster then the expansion of medium. In the case of $n > -2$, one could assume there is nonphysical fluid or the electric conductivity is negative. In this case the fluid contracts in the transverse plane, and the magnetic field decays much slower than the expansion of fluid. We could assume there is a static magnetic field in a medium expanding along the z direction.

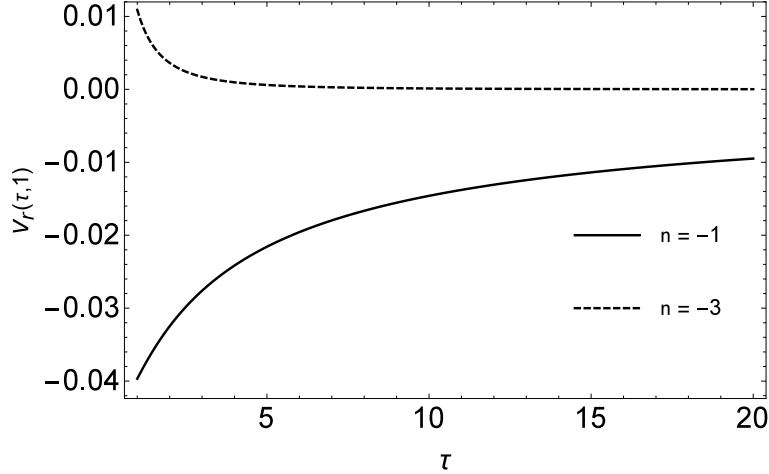


Figure 3: The transverse fluid velocity $v_r(\tau, r)$ is plotted as function of τ for two different values of $n = -1, -3$ at $r = 1$.

Figs 14, and 15 shows the correction energy density in terms of τ or r at either fixed r or fixed τ for the cases $n < -2$ and $n > -2$. According to Fig. 14 and Fig. 15, the correction energy density starting from zero at proper time $\tau = 1$ and for $n > -2$ the correction energy density is negative at any r and τ , while for $n < -2$ the correction energy density is positive at any r and τ . We could interpret above results as follow. For $n > -2$, the fluid contracts, and medium can give an additional contribution energy to the magnetic field. However, in the case $n < -2$ the magnetic field decays fast and the magnetic energy is transferred to the fluid-element according to the energy-conservation law. Besides, the fluid expands radially. In special case $n = -2$ correspond to the situation of the ideal MHD limit in which the evolution of energy density and magnetic field are decoupled which thus results in the absence of transverse flow. In this case the magnetic field decays as $\frac{1}{\tau}$.

3.2 Electromagnetic effect on the spectra

In this subsection we investigate effects of the magnetic field on the particle spectrum. We should notice our model is based on two assumptions, boost invariance along beam line, and rotation invariance in the transverse plane. Thus, we have deduced all quantities of interest only depend on the proper time and the radial coordinate r . Therefore, we do expect our model fit with the experimental data only in mid rapidity and near central collisions. In order to obtain the hadron spectra, we use the Cooper-Frye freeze out prescription over the freeze-out surface [34]:

$$S = E \frac{d^3N}{dp^3} = \frac{dN}{p_T dp_T dy d\varphi} = \int d\Sigma_\mu p^\mu \exp\left(\frac{-p^\mu u_\mu}{T_f}\right) \quad (40)$$

Where T_f is the temperature at the freeze out surface, and u^μ is the 4-velocity of the fluid. The $d\Sigma_\mu$ is the element area on the isothermal freeze out surface in space-time. The freeze out surface is where the temperature of fluid is related to the energy density as $T \propto \epsilon^{1/4}$. It must satisfy $T(\tau, r) = T_f$. In our convention, the area element perpendicular to the freeze out surface is given by:

$$d\Sigma_\mu = (-1, R_f, 0, 0) \tau_f r dr d\varphi d\eta. \quad (41)$$

The integration measure in the Cooper-Frye formula is:

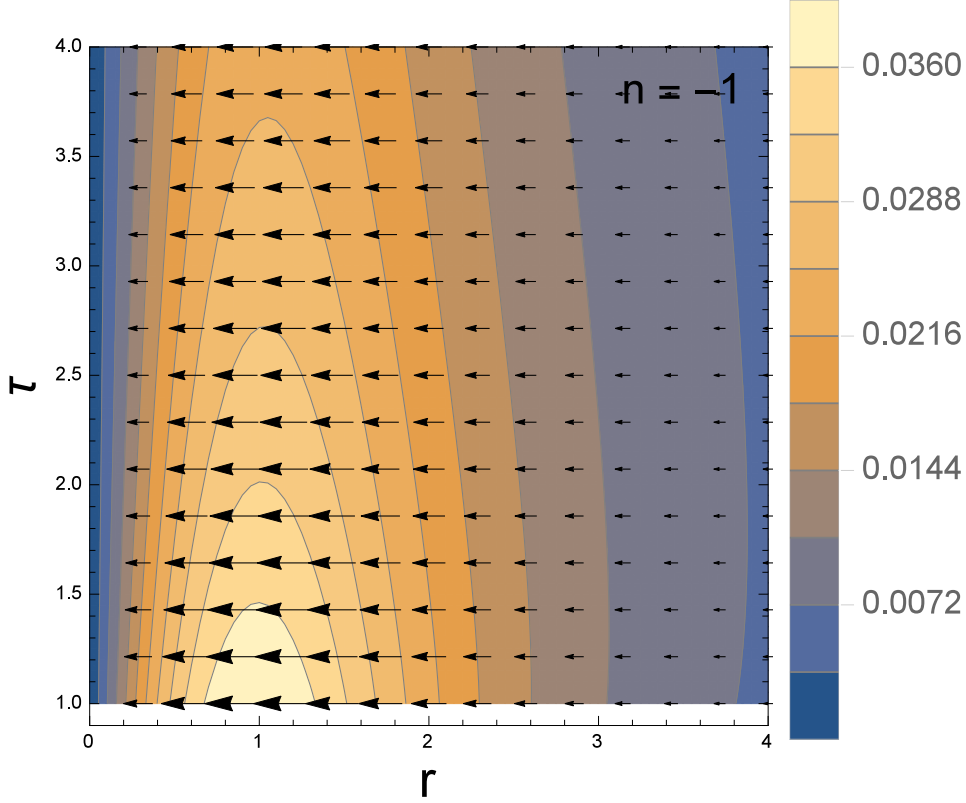


Figure 4: Two-dimensional transverse fluid velocity $v_r(\tau, r)$ is plotted with $n = -1$. The background colors represent the magnitude of v_r .

$$d\Sigma_\mu p^\mu = [-m_T \cosh(Y - \eta) + p_T R_f \cos(\varphi_p - \varphi)] \tau_f dr d\varphi d\eta. \quad (42)$$

Moreover, the scalar product $p^\mu u_\mu$ in the Cooper-Frye formula is

$$p^\mu u_\mu = -m_T \cosh(Y - \eta) u_\tau + p_T \cos(\varphi_p - \varphi) u_r, \quad (43)$$

where $R_f \equiv -\frac{\partial \tau}{\partial r} = \frac{\partial_\tau T}{\partial_r T} |_{T_f}$. Here $\tau = \sqrt{t^2 - z^2}$, r , and $\eta = \frac{1}{2} \log \frac{t+z}{t-z}$, are the longitudinal proper time, the transverse (cylindrical) radius, and the longitudinal rapidity (hyperbolic arc angle), respectively. Similarly u_r is the transverse flow velocity and φ is its azimuthal angle. φ_p is the azimuthal angle in momentum space. Besides, p_T , $m_T = \sqrt{m^2 + p_T^2}$, and Y are the detected transverse momentum, the corresponding transverse mass, and the observed longitudinal rapidity respectively. Thus, the final expression for the CF formula is:

$$S = \frac{g_i}{2\pi^2} \int_0^{x_f} r \tau_f(r) dr \left[m_T K_1\left(\frac{m_T u_\tau}{T_f}\right) I_0\left(\frac{m_T u_r}{T_f}\right) + p_T R_f K_0\left(\frac{m_T u_\tau}{T_f}\right) I_1\left(\frac{m_T u_r}{T_f}\right) \right] \quad (44)$$

Where $\tau_f(r)$ and g_i are the solution of the $T(\tau_f, r) = T_f$, and the degeneracy factor for particles respectively.

The above integral over r on the freeze-out surface is evaluated numerically. Then, the spectra of hadrons is obtained as a function of p_T . The results for the charged pion spectra are presented in Figs. 16 and 17.

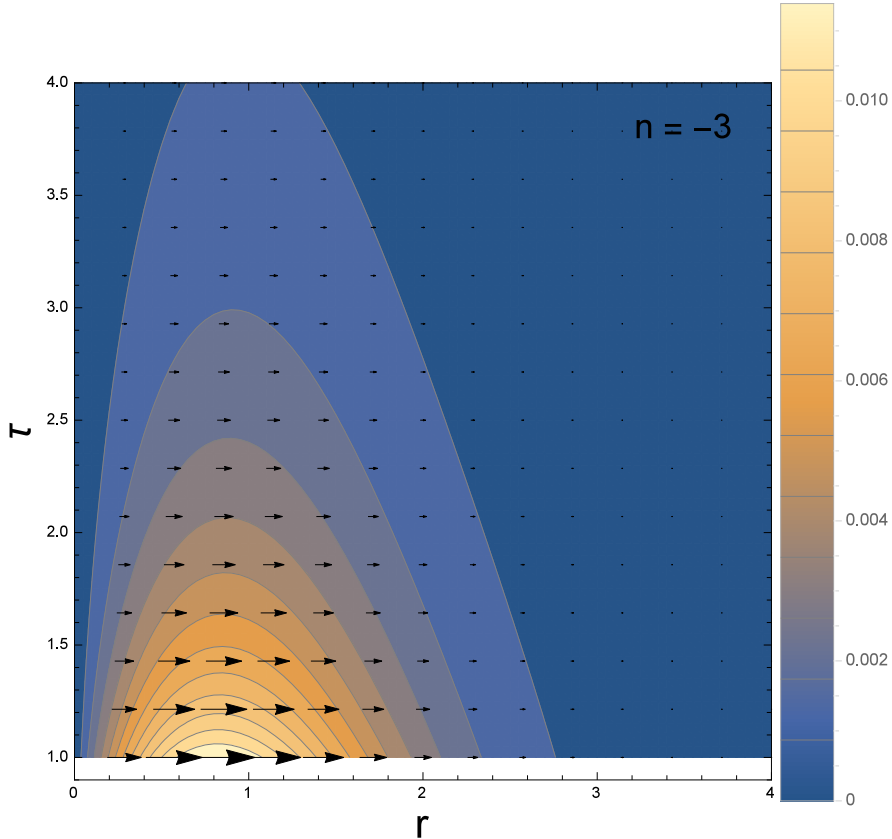


Figure 5: Two-dimensional transverse fluid velocity $v_r(\tau, r)$ is plotted with $n = -3$. The background colors represent the magnitude of v_r .

Figs. 16 and 17 are demonstrated the hadron spectrum of pions. We choose the $T = 130$ MeV isotherm as the freezeout surface in Fig 16 for three different values of the free parameter r_0 . The figure is the comparison of the spectrum of pions (black, bottom) as a function of transverse momentum p_T resulting from our hydrodynamic solution with experimental results for pions (top) obtained at PHENIX [35]. We see the smallest value of r_0 slightly brings the calculation closer to the experimental data. In Fig 16, we choose three different values of the freeze out temperature (140, 150 and 160 MeV) and compared with experimental data at PHENIX [35] in central collisions 0 – 5%.

Our spectra appear to underestimate the experimental data, but their behavior with p_T has the correct trend of a monotonically decrease. The highest value of the freeze out temperature we employed (as suggested, e.g. in Ref. [36]) slightly brings the calculation closer to the experimental data; however it also shows a kind of saturation phenomenon and points to the need of including other effects not considered in the present calculation.

4 Conclusions and outlook

In the present work, we have investigated heavy ion collisions in the presence of a transverse external magnetic field on the special case of a $(1 + 2)$ dimensional longitudinally boost-invariant fluid expansion. We have solved magneto-hydrodynamic equations in presence of a external magnetic

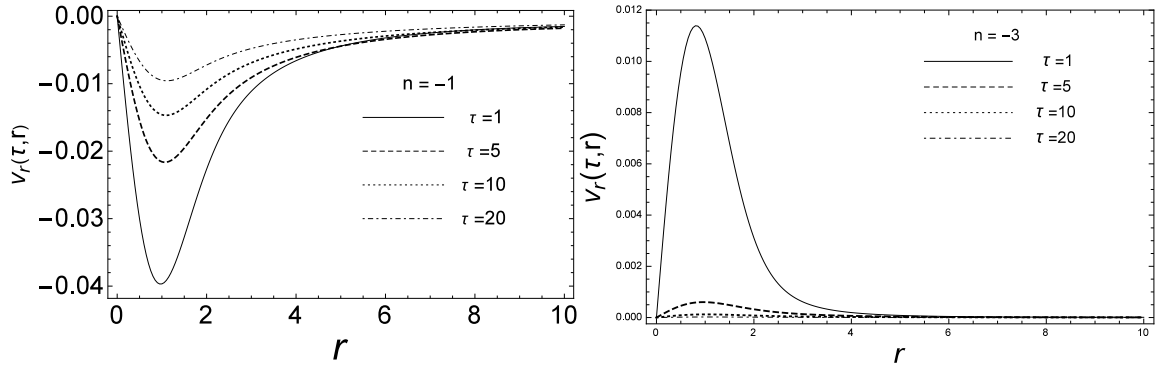


Figure 6: The transverse fluid velocity $v_r(\tau, r)$ in terms of cylindrical radial coordinate r is plotted at different values of proper time τ . Left panel is for $n = -1$ and right panel is for $n = -3$.

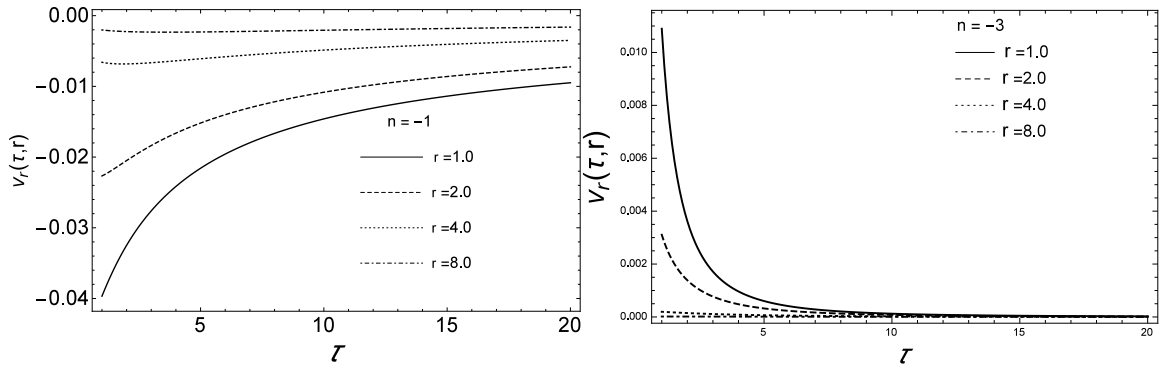


Figure 7: The transverse fluid velocity $v_r(\tau, r)$ is plotted as function of τ at different values of radial coordinate r . Left panel is for $n = -1$ and right panel is for $n = -3$.

field perturbatively. We work in Milne coordinates, and the medium is assumed boost-invariant along the z direction. We remark that in Ref. [28] it been supposed that the external magnetic field is located in the transverse plane as $b_\mu = (0, 0, b_\varphi, 0)$ where $b_\mu b^\mu = b^2$ is defined. Their study was in a simple setup, which includes an azimuthal magnetic field in the matter distribution. In current work we modify the framework, and assume the external magnetic field has two components in transverse plane. Working in cylinder coordinates in transverse plane, we have supposed that $b_\mu = (0, b_r, b_\varphi, 0)$; however, we have assumed that square of the magnetic field only depends on r . This extra assumption simplifies the energy conservation and Euler equations. We have shown that by combining magnetic field with the boost symmetry along the beam direction, a radial flow perpendicular to the beam axis is created and the energy density of the fluid is altered. Although we have chosen the Gaussian distribution as one particular example for the space-dependent magnetic field, the same approach can be applied to other spatial distribution which can be approximated by a series of Bessel functions. Since the analytic expressions of each moment is found, one can directly compute the transverse velocity and correction on energy density by just inputting the Bessel coefficients of series. The energy conservation and Euler equations reduced to two coupled differential equations, which could be solved analytically in the weak-field approximation. We have demonstrated in detail how the fluid velocity and energy density are modified by the magnetic field. For the solutions obtained by our numerical calculations we have assumed an initial energy density

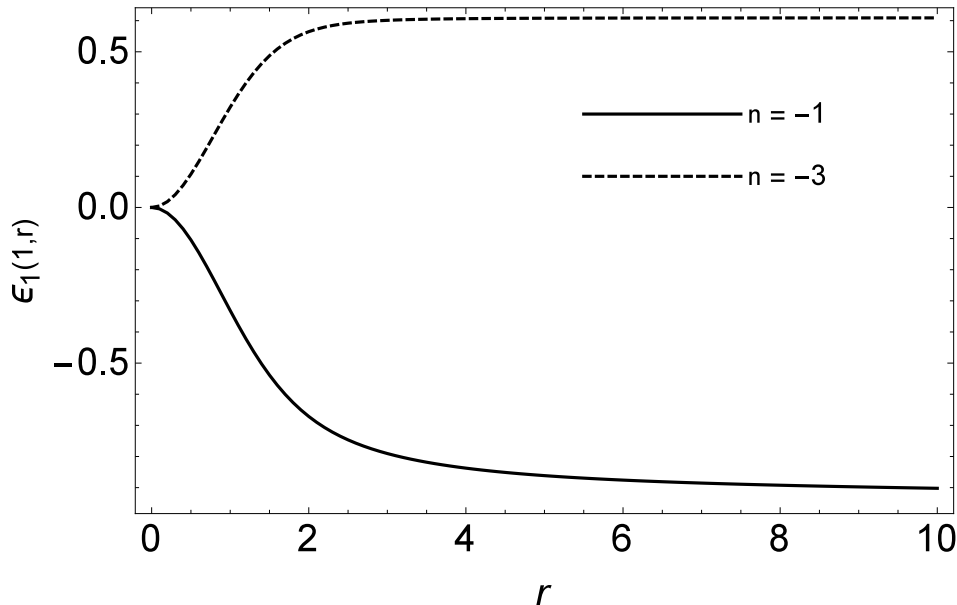


Figure 8: The correction of energy density $\epsilon_1(\tau, r)$ (GeV/fm^3) in terms of cylindrical radial coordinate r is plotted for two different values of $n = -1, -3$ at $\tau = 1$.

of the fluid at time $\tau = 1$ fixed to $B^2/\epsilon_c = 0.6$. We have considered different decays with time of the magnetic field: $\tau^n/2$, with $n < 0$. A visual presentation of the flow for $n = -1$ and $n = -3$ can be found in Figs. 2 and 3 and for different values of n in Figs. 12 and 13.

We stress that the present work presents an approximated calculation which can be useful for cross checking current and future numerical calculations in some limiting region. Indeed, the effect of such a scenario on hadronic flow in heavy ion collisions requires more pragmatic debates. Moreover our perturbative solutions could be used as initial conditions in the late time for future numerical calculations.

References

- [1] R. Andrade, F. Grassi, Y. Hama, T. Kodama, O. Socolowski Jr., “On the necessity to include event-by-event fluctuations in experimental evaluation of elliptical flow”, *Phys. Rev. Lett.* **97**, 202302 (2006).
- [2] P. Romatschke, U. Romatschke, “Viscosity information from relativistic nuclear collisions: how perfect is the fluid observed at RHIC?”, *Phys. Rev. Lett.* **99**, 172301 (2007).
- [3] H. Song, U.W. Heinz, “Causal viscous hydrodynamics in 2+1 dimensions for relativistic heavy-ion collisions”, *Phys. Rev. C* **77**, 064901 (2008).
- [4] P. Bozek, “Flow and interferometry in 3+1 dimensional viscous hydrodynamics”, *Phys. Rev. C* **85**, 034901 (2012).
- [5] C. Gale, S. Jeon, B. Schenke, P. Tribedy, R. Venugopalan, “Event-by-event anisotropic flow in heavy-ion collisions from combined Yang-Mills and viscous fluid dynamics”, *Phys. Rev. Lett.* **110**(1), 012302 (2013).
- [6] L. Del Zanna, et al., “Relativistic viscous hydrodynamics for heavy-ion collisions with ECHO-QGP”, *Eur. Phys. J. C* **73**, 2524 (2013).

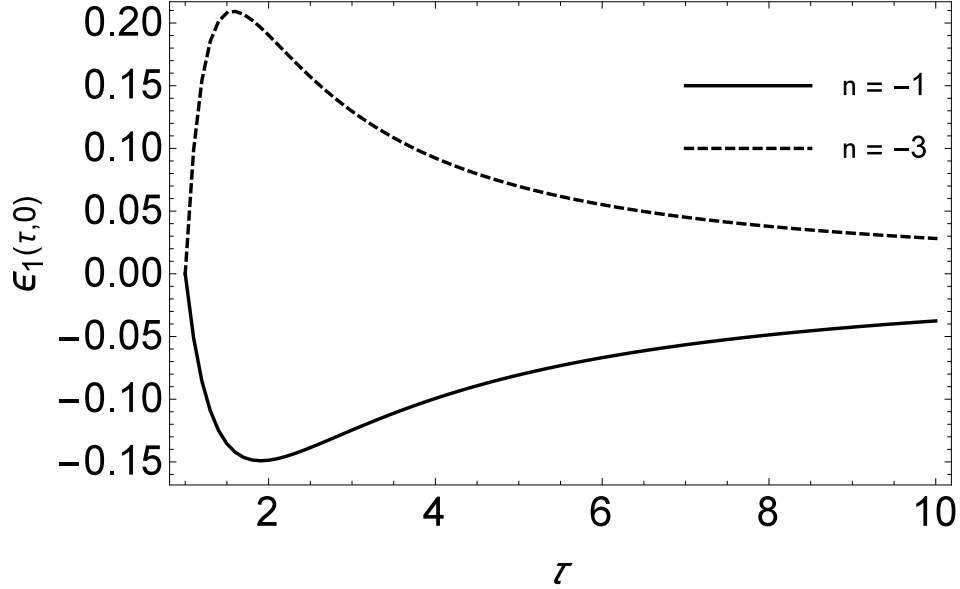


Figure 9: The correction of energy density $\epsilon_1(\tau, r)$ (GeV/fm^3) is plotted as function of τ for two different values of $n = -1, -3$ at $r = 0$.

- [7] J. Rafelski, B. Muller, “Magnetic splitting of quasimolecular electronic states in strong fields”, Phys. Rev. Lett. 36, 517 (1976).
- [8] D. E. Kharzeev, L. D. McLerran, H. J. Warringa, “The effects of topological charge change in heavy ion collisions: Event by event P and CP violation”, Nucl. Phys. A 803, 227 (2008).
- [9] Y. Zhong, C. B. Yang, X. Cai, S. Q. Feng, “A systematic study of magnetic field in Relativistic Heavy-ion Collisions in the RHIC and LHC energy regions”, Adv. High Energy Phys. 2014, 193039 (2014).
- [10] K. Fukushima, D. E. Kharzeev, H. J. Warringa, “The chiral magnetic effect”, Phys. Rev. D 78, 074033 (2008).
- [11] D. E. Kharzeev and H. U. Yee, “Chiral magnetic wave”, Phys. Rev. D 83, 085007 (2011).
- [12] Y. Burnier, D. E. Kharzeev, J. Liao, H. U. Yee, “Chiral magnetic wave at finite baryon density and the electric quadrupole moment of quark-gluon plasma in heavy ion collisions”, Phys. Rev. Lett. 107, 052303 (2011).
- [13] X. G. Huang, J. Liao, “Axial current generation from electric field: chiral electric separation effect”, Phys.Rev.Lett. 110, 232302 (2013).
- [14] S. Pu, S. Y. Wu, D. L. Yang, “Holographic chiral electric separation effect”, Phys. Rev. D 89, 085024 (2014).
- [15] Y. Jiang, X. G. Huang, J. Liao, “Chiral electric separation effect in the quark-gluon plasma”, Phys. Rev. D 91, 045001 (2015).
- [16] S. Pu, S. Y. Wu, D. L. Yang, “Chiral Hall effect and chiral electric waves”, Phys. Rev. D 91, 025011 (2015).

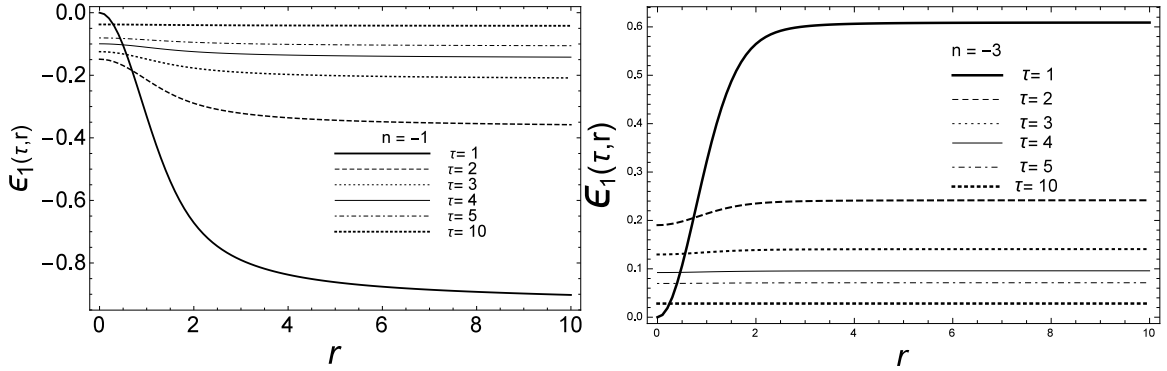


Figure 10: The correction energy density ϵ_1 (GeV/fm^3) is plotted as a function of radial coordinate r for different values of τ . Left panel $n = -1$ and right panel $n = -3$.

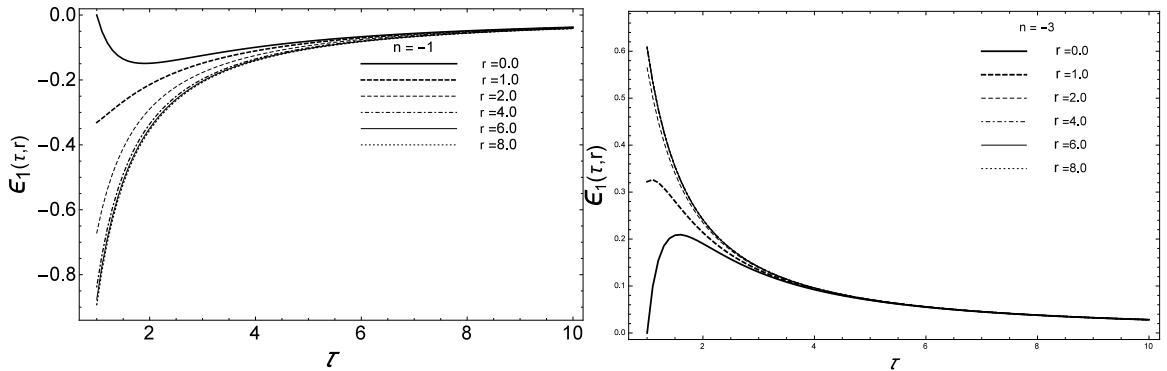


Figure 11: The correction energy density ϵ_1 (GeV/fm^3) as a function of proper time τ for different values of radial coordinate r . Left panel $n = -1$ and right panel $n = -3$.

- [17] K. Tuchin, “Time and space dependence of the electromagnetic field in relativistic heavy-ion collisions”, *Phys. Rev. C* 88, 024911 (2013).
- [18] U. Gürsoy, D. Kharzeev, K. Rajagopal, “Magneto-hydrodynamics, charged currents, and directed flow in heavy-ion collisions”, *Phys. Rev. C* 89, 054905 (2014).
- [19] B.G. Zakharov, “Electromagnetic response of quark-gluon plasma in heavy-ion collisions”, *Phys. Lett. B* 737, 262–266 (2014).
- [20] H. Li, X. L. Sheng, Q. Wang, “Electromagnetic fields with electric and chiral magnetic conductivities in heavy-ion collisions”, *Phys. Rev. C* 94, 044903 (2016).
- [21] G. Inghirami, L. Del Zanna, A. Beraudo, M. Haddadi Moghaddam, F. Becattini, M. Bleicher, “Numerical magneto-hydrodynamics for relativistic nuclear collisions”, *Eur. Phys. J. C* 76, 659 (2016).
- [22] M. Greif, C. Greiner, Z. Xu, “Magnetic field influence on the early time dynamics of heavy-ion collisions”, *Phys. Rev. C* 96, 014903 (2017).
- [23] M. H. Moghaddam, B. Azadegan, A. F. Kord, W. M. Alberico, “Non-relativistic approximate

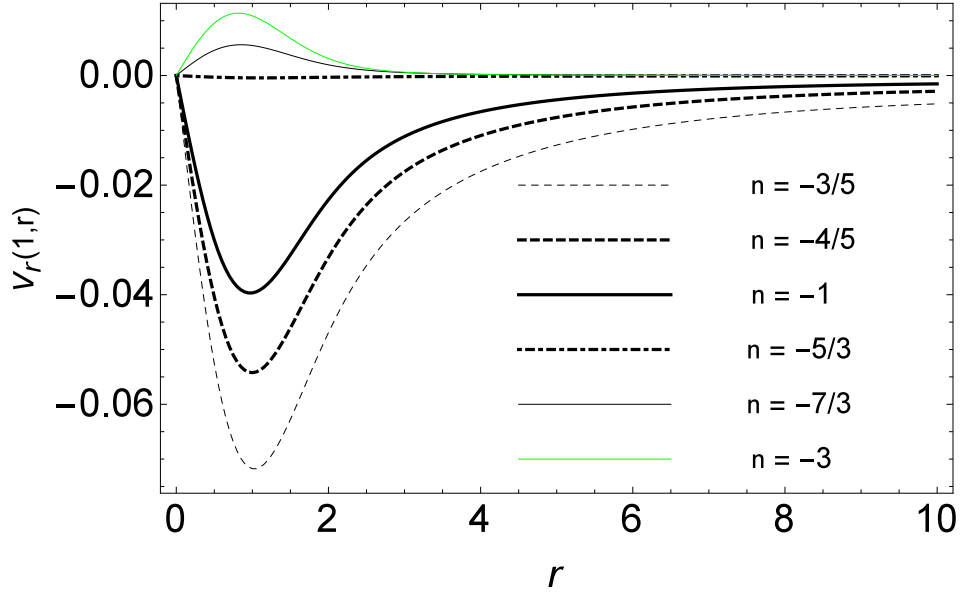


Figure 12: The fluid velocity $v_r(\tau, r)$ is plotted in terms of r at $\tau = 1$ with different values of n .

numerical ideal-magneto-hydrodynamics of (1+1D) transverse flow in Bjorken scenario”, Eur. Phys. J. C 78, 255 (2018).

- [24] G. Inghirami, M. Mace, Y. Hirono, L. Del Zanna, D. E. Kharzeev, M. Bleicher, “Magnetic fields in heavy-ion collisions: flow and charge transport”, Eur. Phys. J. C 80, 293 (2020).
- [25] V. Roy, S. Pu, L. Rezzolla, D. Rischke, “Analytic Bjorken flow in one-dimensional relativistic magneto-hydrodynamics”, Phys. Lett. B 750, 45 (2015).
- [26] S. Pu, V. Roy, L. Rezzolla, D. H. Rischke, “Bjorken flow in one-dimensional relativistic magneto-hydrodynamics with magnetization”, Phys. Rev. D 93, 074022 (2016).
- [27] S. Pu, D. L. Yang, “Transverse flow induced by inhomogeneous magnetic fields in the Bjorken expansion”, Phys. Rev. D 93, 054042 (2016).
- [28] M. H. Moghaddam, B. Azadegan, A. F. Kord, W. M. Alberico, “Transverse expansion of hot magnetized Bjorken flow in heavy ion collisions”, Eur. Phys. J. C 79, 619 (2019).
- [29] V. Roy, S. Pu, L. Rezzolla, and D. H. Rischke, “Effect of intense magnetic fields on reduced magneto-hydrodynamics evolution in $\sqrt{s_{NN}} = 200$ GeV Au + Au collisions”, Phys. Rev. C 96, 054909 (2017).
- [30] L. Rezzolla, O. Zanotti, “Relativistic Hydrodynamics”, Oxford University Press (2013).
- [31] A. M. Anile, “Relativistic fluids and magneto-fluids”, Cambridge University Press, Cambridge, (1989).
- [32] J. Goedbloed, R. Keppens, S. Poedts, “Advanced magneto-hydrodynamics with applications to laboratory and astrophysical plasmas”, Cambridge University Press, Cambridge (2010).
- [33] D. Teaney, “Effect of shear viscosity on spectra, elliptic flow, and Hanbury Brown–Twiss radii”, Phys. Rev. C 68, 034913 (2003).

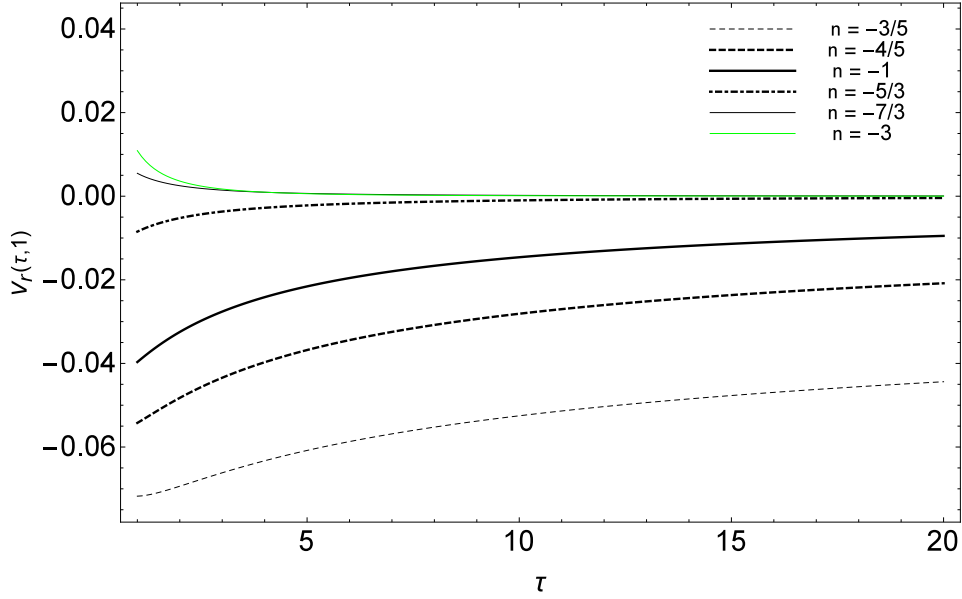


Figure 13: The fluid velocity $v_r(\tau, r)$ in terms of τ plot at $r = 1$ with different values of n .

- [34] F. Cooper and G. Frye, Phys. Rev. D 10, 186 (1974).
- [35] K. Adcox et al., (PHENIX Collaboration), Formation of dense partonic matter in relativistic nucleusnucleus collisions at RHIC: Experimental evaluation by the PHENIX Collaboration. Nucl. Phys. A 757, 184 (2005)
- [36] C. Ratti, R. Bellwied, J. Noronha-Hostler, P. Parotto, I. Portillo Vazquez, J.M. Stafford. arXiv:1805.00088 [hep-ph]

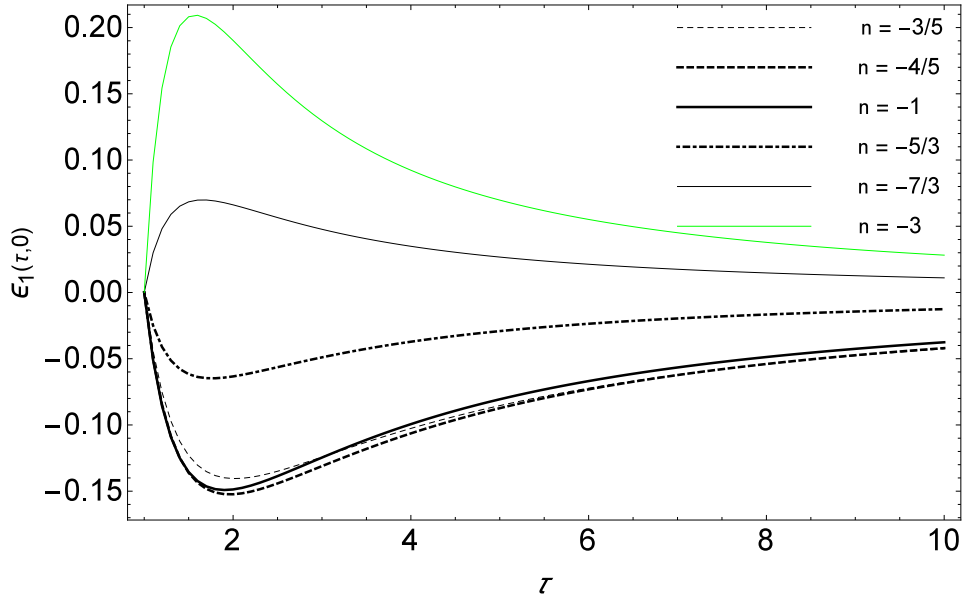


Figure 14: The correction energy density $\epsilon_1(\tau, r)$ (GeV/fm^3) is plotted in terms of τ at $r = 0$ with different values of n .

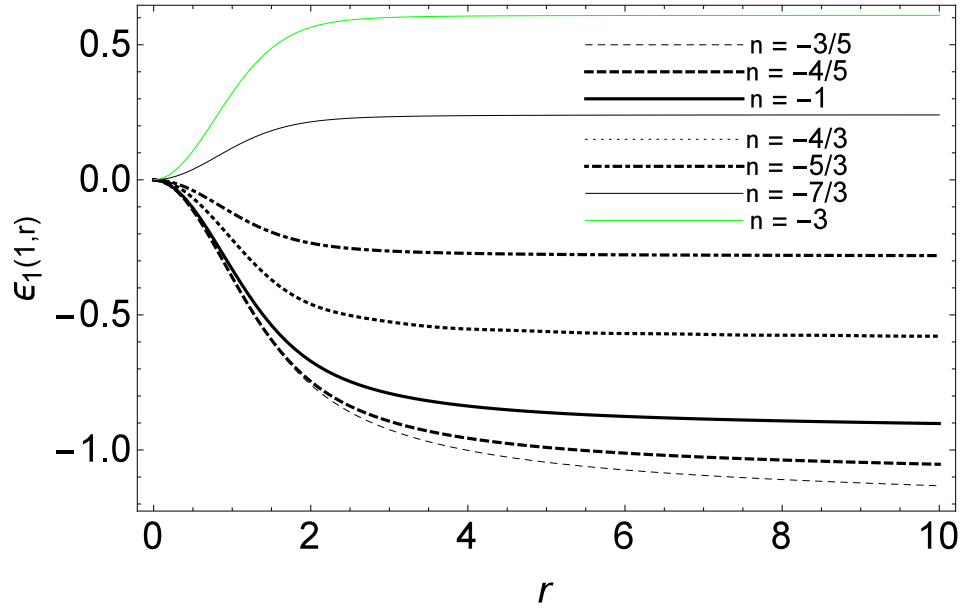


Figure 15: The correction energy density $\epsilon_1(\tau, r)$ (GeV/fm^3) is plotted in terms of r at $\tau = 1$ with different values of n .

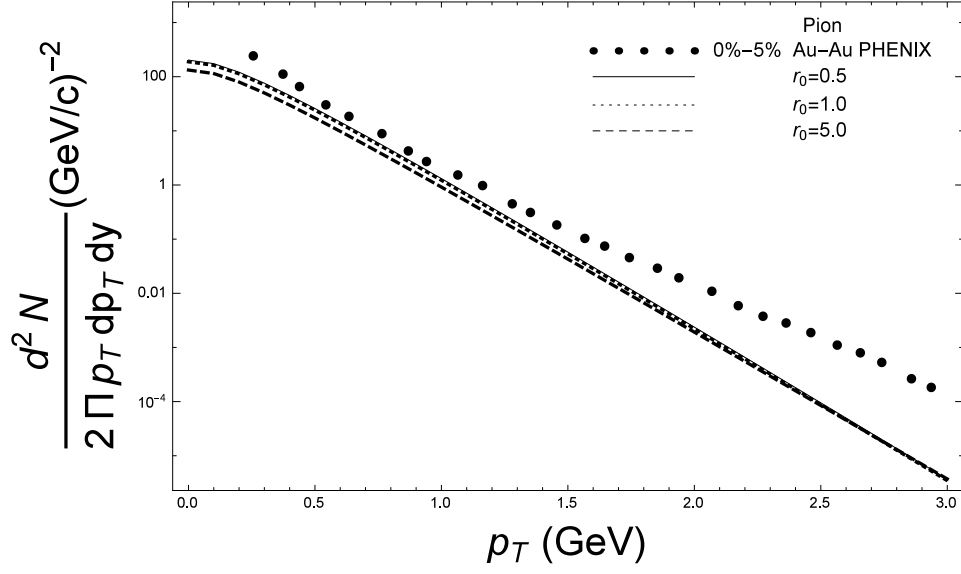


Figure 16: Pion transverse spectrum from central Au-Au collisions with value of $n = -1$. The black solid, thin dashed, and thick dashed lines are corresponded to $r_0 = 0.5, 1$ and 5 , respectively. Black dot line is PHENIX data.

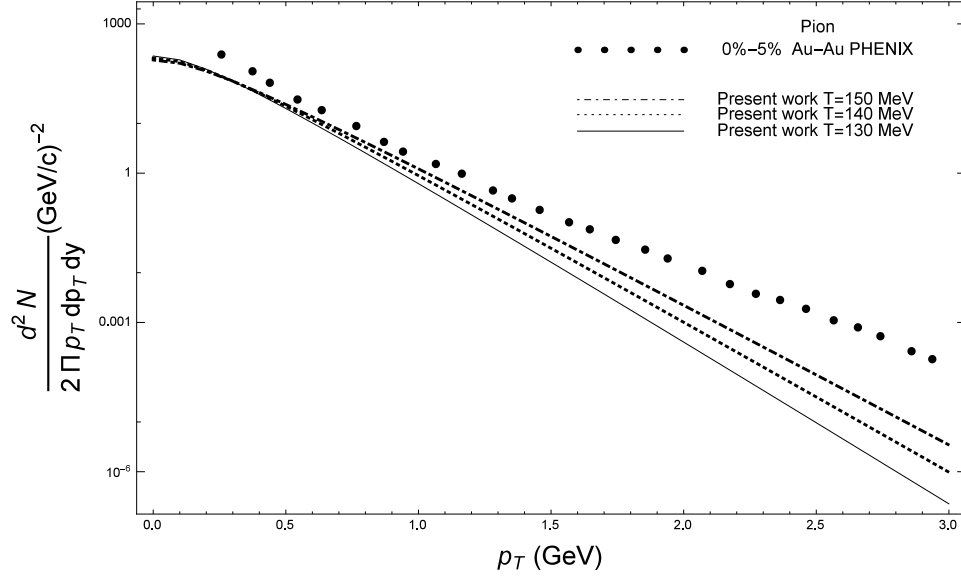


Figure 17: Pion transverse spectrum from central Au-Au collisions with value of $n = -1$. The black solid, dashed, and dash-dotted lines are corresponded to a freeze out temperature of $140, 150$ and 160 MeV, respectively. The black dots are PHENIX data.